ACS OMEGA

Open Access



http://pubs.acs.org/journal/acsodf

Article

# TRIP13 Plays an Important Role in the Sensitivity of Leukemia Cell Response to Sulforaphane Therapy

Lei Liu,[▽] Baixue Liao,[▽] Ruiling Fan, Yanxia Liu, Aoshuang Li, Lüye Liu, Yan Li,* and Jing Li*

Cite This: *ACS Omega* 2024, 9, 26628−26640

Read Online

ACCESS | Metrics & More | Article Recommendations | Supporting Information

**ABSTRACT:** Sulforaphane is one of the most characterized isothiocyanate compounds in cruciferous vegetables and shows anticancer effects, especially antileukemia properties. However, the molecular mechanism of the growth inhibition effect of sulforaphane in acute myeloid leukemia (AML) has not been fully explored. In the present study, a proteomic analysis was performed on the AML cell line U937 responding to sulforaphane treatment to identify novel and efficient therapeutic targets of sulforaphane on AML cells. Key driver analysis was run on the leukemia network, and TRIP13 was identified as a key regulatory factor in sulforaphane-induced growth inhibition in U937 cells. Pretreatment with DCZ0415, an inhibitor of TRIP13, could significantly attenuate sulforaphane-induced cell apoptosis and cell cycle arrest in vitro through the PI3K/Akt/mTOR signaling pathway. In addition, the inhibitory effect of sulforaphane on the tumor volume could also be obviously attenuated by the pretreatment of DCZ0415 in vivo. These results indicate that TRIP13 plays an important role in the sensitivity of leukemia cell response to sulforaphane treatment, and these findings expand the understanding of the mechanism of the antileukemic effect of sulforaphane and provide a new target for the treatment of AML.

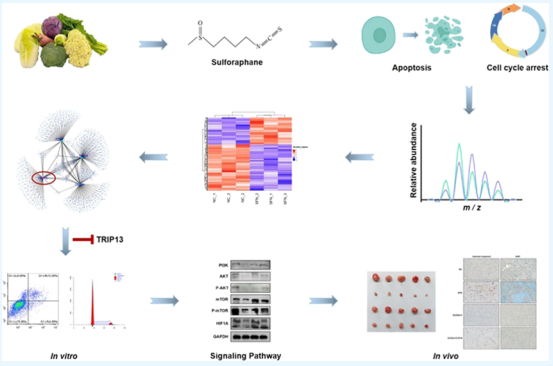


## 1. INTRODUCTION

Sulforaphane (SFN), 1-isothiocyanato-4-methylsulfinyl-butane, is an isothiocyanate found in cruciferous vegetables, which is one of the most characterized isothiocyanate compounds and has shown anticancer properties. Recent studies demonstrated that SFN acted as a therapeutic agent in various cancers[1−5] and especially played an important role in the treatment of leukemia.[6−8] Acute myeloid leukemia (AML) is a hematologic malignancy with high mortality rates, and it is a heterogeneous disease characterized by blocked differentiation and uncontrolled proliferation of blasts.[9] Because of the self-renewal capability of leukemia stem cells, there is a high relapse ratio in AML. Despite marked improvements in AML management, the outcomes are still unsatisfactory. It is still a great challenge to seek more effective approaches to AML treatment.

At present, some studies have been conducted on the mechanism of the growth inhibition effect of SFN in AML. Sulforaphane could induce apoptosis in human leukemia HL-60 cells through extrinsic and intrinsic signal pathways.[10] SFN also could induce nonapoptotic cell death modalities. SFN triggered different cell death modalities in a dose-dependent manner. At 25 $\mu$M, SFN induced caspase-dependent apoptosis, and at 50 $\mu$M, ferroptosis was induced through depletion of glutathione (GSH), decreased GSH peroxidase 4 protein expression, and lipid peroxidation. In contrast, necroptosis was not involved in SFN-induced cell death.[11] Some microRNAs were reported in AML pathogenesis and as therapeutic targets in SFN-induced cell apoptosis. The miR-155 level was significantly higher in patients with AML compared to controls, and the anticancer effects of sulforaphane can be correlated with the reduction of miR-155 levels. Sulforaphane could induce more differentiation in myeloid progenitor cells by controlling the miR-155, thereby mitigating the progress of AML.[12] MiR-181a levels contribute to AML pathogenesis, and thus, it can be considered as a strategy to control AML progression in patients. SFN could arrest cell proliferation and induce apoptosis in AML cell lines by retarding the expression of miR-181a and affecting the miR-181a pathway, which already clarified its role in the differentiation of hematopoietic stem cells and indicates another mode of anticancer action of SFN.[6] SFN could also inhibit the proliferation of leukemia stem-like cells in vitro and in vivo. After SFN treatment, the expression of the key players in the Sonic Hedgehog (Shh) signaling pathway was significantly decreased at transcriptional and protein levels. Consistent with this, SFN suppressed proliferation in Shh-overexpressed cells more than in Shh-downregulated cells, suggesting that SFN negatively modulates the proliferation of leukemia stem-like cells by affecting the

**Received:** April 10, 2024
**Revised:** May 22, 2024
**Accepted:** May 29, 2024
**Published:** June 6, 2024

Shh signaling pathway.[8] However, to date, the molecular mechanism of the SFN-induced proliferation inhibition in AML cells has not been fully explored, and it is still needed to find novel and efficient therapeutic targets.

As proteins are molecules that ultimately perform biological functions, in the present study, the proteomic analysis was performed on the AML cell line U937 responding to SFN treatment to find more clues to decipher how SFN could induce growth inhibition of AML cells. Proteomic expression profiling showed that a total of 238 proteins were identified as differentially expressed proteins (DEPs) from the control U937 cell compared to that with SFN treatment. Key driver analysis was run on the leukemia network, and thyroid hormone receptor interacting protein 13 (TRIP13) was identified as a key regulatory factor in SFN-induced apoptosis and cell cycle arrest in U937 cells. Previous research reported that TRIP13 plays a key role in regulating mitotic processes, including the spindle assembly checkpoint and DNA repair pathways, which may account for chromosome instability (CIN). As CIN is a predominant hallmark of cancer, TRIP13 may act as a tumor susceptibility locus. Amplification of TRIP13 has been observed in various human cancers and implicated in several aspects of malignant transformation, including cancer cell proliferation, drug resistance, and tumor progression, so TRIP13 has significant potential for cancer treatment.[13] However, the role of TRIP13 in the progression and treatment of AML is still unclear. Therefore, in the present study, we investigated whether TRIP13 is a key factor in SFN-induced growth inhibition in AML cells in vitro and in vivo. These findings have expanded the understanding of the mechanism of the antileukemic effect of SFN and provided a new target for the treatment of AML.

## 2. MATERIAL AND METHODS

**2.1. Cell Culture.** The human acute myeloid leukemia cell line U937 was obtained from the American Type Culture Collection (ATCC, VA) and cultured in RPMI 1640 medium supplemented with 10% fetal bovine serum (FBS), 100 U/mL penicillin, and 100 $\mu$g/mL streptomycin. Cells were incubated in fresh medium at a starting concentration of $2 \times 10^5$ cells/mL and fresh medium was added every 2 to 3 days to maintain the cell density between $2 \times 10^5$ and $1 \times 10^6$ cells/mL at 37 °C with 5% $CO_2$.

**2.2. Reagents and Antibodies.** SFN was purchased from Sigma (MO) and dissolved in dimethyl sulfoxide (DMSO) to prepare a stock solution (40 mM) and stored at −20 °C. DCZ0415, the inhibitor of TRIP13, was purchased from MCE (NJ) and dissolved in DMSO to prepare a stock solution with a concentration of 2.5 mM and stored at −20 °C. Antibodies against cleaved-PARP, cleaved-caspase-3, cyclin D1, cyclin A2, c-Myc, phospho-cdc2, CDK2, PI3K, Akt, phospho-Akt, mTOR, phospho-mTOR, and HIF-1$\alpha$ were purchased from Cell Signaling Technology (MA), and antibodies against TRIP13 and GAPDH were purchased from Proteintech (Wuhan, China).

**2.3. Viability Assay.** The U937 cells were plated into 96-well plates ($5 \times 10^4$ cells/well) and treated with SFN at concentrations of 0−40 $\mu$M for 24 h. Cell inhibition rates were measured using a Cell Counting Kit-8 (CCK-8) (Dojindo Laboratories, Japan) according to the manufacturer's instructions. The absorbance was measured by an EnSpire Multimode Plate Reader (PerkinElmer, CA) at 450 nm. The experiment was performed three times independently.

**2.4. Apoptosis Assay.** The U937 cells were plated into 24-well plates ($5 \times 10^5$ cells/mL) and treated with SFN at concentrations of 0, 10, 20, 30, and 40 $\mu$M for 24 h or at 40 $\mu$M for 0, 6, 12, 24, and 48 h. The apoptotic cells were identified by Alexa Fluor647-conjugated Annexin V/propidium iodide (PI) staining (Solarbio Life Sciences, Beijing, China) according to the manufacturer's instructions. Flow cytometry analysis was performed with a CytoFLEX flow cytometer (BECKMAN COULTER, CA). Both early apoptotic (Annexin V-positive, PI-negative) and late apoptotic (Annexin V-positive and PI-positive) cells were defined as apoptotic cells.

**2.5. Cell Cycle Analysis.** The U937 cells were plated into 6-well plates ($5 \times 10^5$ cells/mL) and treated with SFN at concentrations of 0−40 $\mu$M for 24 h or at 40 $\mu$M for 0−48 h. The cells were harvested and fixed at 4 °C in 70% ethanol for 24 h. After fixation, the cells were incubated with RNase A and propidium iodide (PI) dye (Beyotime, Jiangsu, China) according to the manufacturer's instructions. Finally, the fluorescence intensity of the PI-DNA complex was measured by CytoFLEX flow cytometer (Beckman Coulter, CA). The distribution of cells in different stages of the cell cycle was analyzed by Modfit LT4.0 software.

**2.6. Western Blotting.** The treated cells were harvested at indicated concentrations and appointed time points. Cells were lysed in radioimmunoprecipitation assay (RIPA) lysis buffer (Beyotime, Jiangsu, China), which contained a protease inhibitor cocktail (Roche, Mannheim, Germany). Protein concentrations were determined using a bicinchoninic acid (BCA) protein assay reagent (Thermo, MA). Equal amounts of cell lysate were loaded onto sodium dodecyl-sulfate polyacrylamide gel electrophoresis (SDS-PAGE) gels and then transferred to polyvinylidene fluoride (PVDF) membranes. Membranes were blocked with 5% fat-free milk and incubated with the indicated primary antibodies at 4 °C overnight. The membranes were incubated with horseradish peroxidase-conjugated species-specific secondary antibodies (Cell Signaling Technology, MA). Bands were visualized with enhanced chemiluminescence reagent (Millipore, MA) and imaged by a ChemiDoc MP imaging system (Bio-Rad, MA).

**2.7. Protein Digestion.** Two groups of U937 cells (control and SFN-treated cells; each group contained three samples) were used for label-free liquid chromatography-tandem mass spectrometry (LC-MS/MS) assays. Total proteins were extracted by using a urea lysis buffer containing 8 M urea, 1% SDS, and the protease inhibitor cocktail. Proteins were quantified using the BCA assay kit (Thermo Scientific, IL) and detected by SDS-PAGE. Total proteins were treated following tris(2-carboxyethyl)phosphine (TCEP) reduction, Iodoacetamide alkylation, and trypsin digestion to obtain peptides. Then, equal amounts of peptides from six samples were desalted using a C18 solid-phase extraction and subjected to LC-MS/MS analysis.

**2.8. LC-MS/MS.** The peptides of each sample were separated on the EASY-nLC 1200 high-performance liquid chromatography (HPLC) system using a C18 column (75 $\mu$m × 25 cm) (Thermo Scientific) over a 120 min gradient from buffer A (2% acetonitrile and 0.1% formic acid, vol/vol) and B linear gradient solvent (80% acetonitrile and 0.1% formic acid) at a flow rate of 300 nL/min. Peptides eluting from the column were analyzed by MS/MS using a quadrupole-Orbitrap mass Spectrometer (Q-Exactive) (Thermo Scientific) equipped with an online nanoelectrospray ion source. MS/MS spectra were


https://doi.org/10.1021/acsomega.4c03450
ACS Omega 2024, 9, 26628−26640

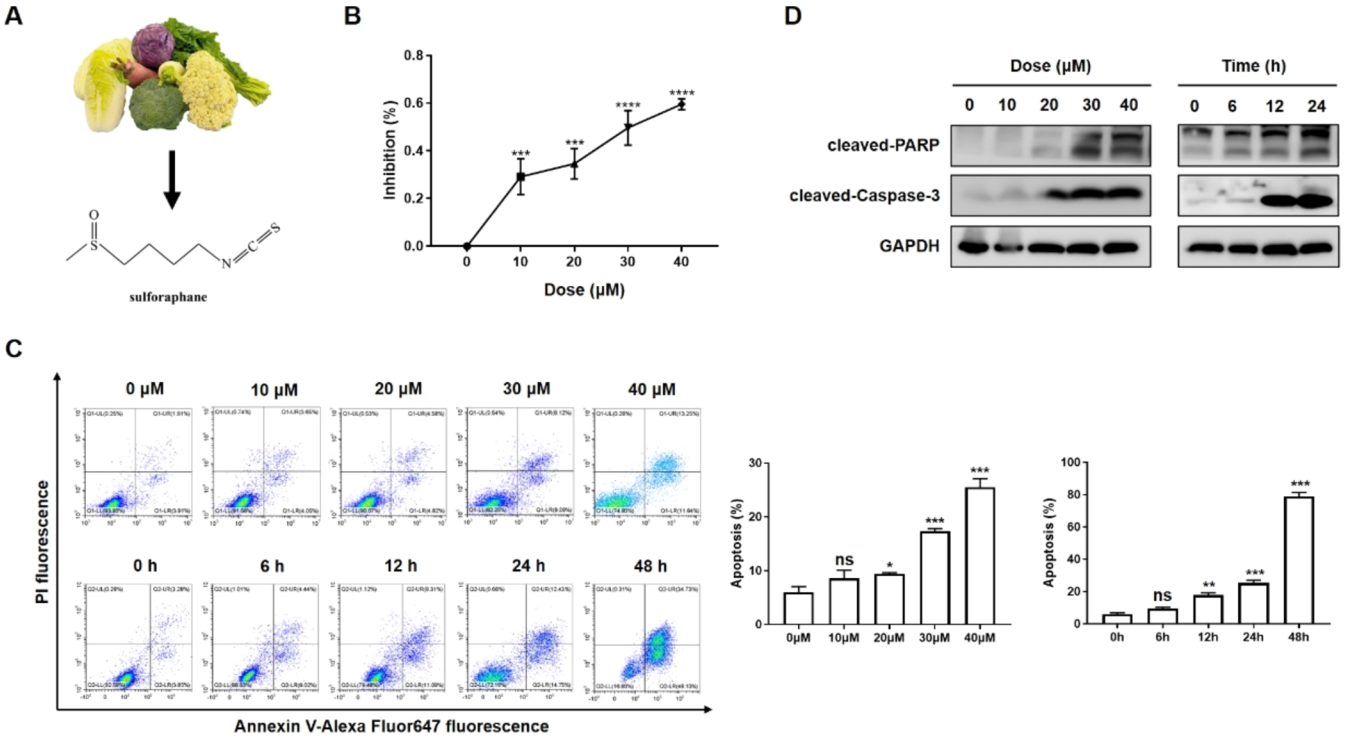


**Figure 1.** SFN-inhibited cell growth and induced apoptosis in the leukemia cell line U937. (A) Chemical structure of SFN. (B) Growth inhibition effect of SFN analyzed at indicated concentrations for 24 h in U937 cells. (C) Cells treated with SFN at indicated concentrations for 24 h or treated with 40 $\mu$M SFN for indicated durations. The percentage of apoptotic cells was determined by fluorescence-activated cell sorting (FACS) analysis (left panel), and the bar chart displays the statistical analysis results of the cell apoptosis ratio (right panel). (D) The expression of apoptosis-related proteins analyzed by immunoblotting. Each experiment was repeated three times. *$P$ < 0.05, **$P$ < 0.01, ***$P$ < 0.001, and ****$P$ < 0.0001.

acquired by data-dependent acquisition (DDA) in full scan mode ($m/z$ 350−1300) with a mass resolution of 70,000, followed by 20 sequential high-energy collisional dissociation MS/MS scans with a resolution of 175,000. In all cases, one micro scan was recorded using dynamic exclusion of 60 s.

**2.9. Data Calculation and Analysis.** The original LC-MS/MS files were imported into MaxQuant for library checking and an unlabeled quantitative analysis using the database uniprot-proteome_UP000005640-*Homo sapiens*-20170619-71913s.fasta. MS data were analyzed using PEAKS Studio software version 8.5 (Bioinformatics Solutions Inc., Waterloo, Canada), and the parameters were set up as follows: dynamic modification (methionine oxidation and protein N-terminal acetylation), static modification (carbamidomethylation of cysteines), enzyme (trypsin), maximum missed cleavages per peptide (2), precursor mass tolerance (10 ppm), and fragment mass tolerance (0.05 Da). The result-filtering parameter is peptide false discovery rate (FDR) ≤ 0.01. Statistical analysis was performed using the $t$ test. A fold change of <0.67 or >1.5 and $P$ < 0.05 were defined as significantly different in this study.

**2.10. Bioinformatics Analysis.** The identified proteins with $P$ values <0.05 and $\log_2$|fold change| ≥ 0.58 between two groups were considered as differentially expressed proteins (DEPs). The hierarchical clustering analysis of the DEPs was performed using hcluster (https://pypi.python.org/pypi/hcluster/0.2.0). The expression patterns of upregulated and downregulated proteins were analyzed by a clustering assay. To reveal the functions of the DEPs, we performed Gene Ontology (GO) annotation and pathway analysis. In brief, GO annotation was analyzed based on the DAVID database (https://david.ncifcrf.gov/tools.jsp) to discover the gene regulatory networks based on hierarchical categories according to the molecular function (MF), biological process (BP), and cellular component (CC) terms of the DEPs. Pathway analysis was performed with the Kyoto Encyclopedia of Genes and Genomes (KEGG) (http://www.genome.jp/kegg/), Panther, WikiPath, and BioCarta database. Enriched GO and pathway terms with $P$-value <0.05 were considered as statistically significant, and bubble plots were implemented with the ggplot2 package (https://ggplot2.tidyverse.org/) in an R language environment. The protein−protein interaction (PPI) of DEPs was conducted on the String (http://string-de.org/, version 10.0), and the PPI network topology was analyzed by using Cytoscape software (http://www.cytoscape.org/). The key driver analysis (KDA) was run on the leukemia network by using the KDA package in R.

**2.11. Animal Experiments.** To investigate the inhibitory effect of SFN on U937 cell growth in vivo and the role of TRIP13 in the SFN-mediated antitumor effect, a xenograft nude mice model was constructed. Briefly, the mice were divided into four groups (NC, SFN, DCZ0415, and DCZ0415 + SFN group). In DCZ0415 and DCZ0415 + SFN groups, DCZ0415 was injected intraperitoneally 1 week before xenograft inoculation to inhibit the expression of TRIP13 in vivo, and phosphate buffered saline (PBS) was injected as the control in NC and SFN groups. Then, $2 \times 10^6$ U937 cells were resuspended in a 1:1 ratio (total volume: 100 $\mu$L) in PBS with a Matrigel basement membrane matrix and subcutaneously injected into the right dorsal flank in the mice. After 1 week of injection, the mice were treated with SFN in the SFN group and DCZ0415 + SFN group for 2 weeks. PBS and DCZ0415 were injected continuously in the NC group and DCZ0415 group, respectively. Tumor sizes were measured with calipers


https://doi.org/10.1021/acsomega.4c03450
ACS Omega 2024, 9, 26628−26640

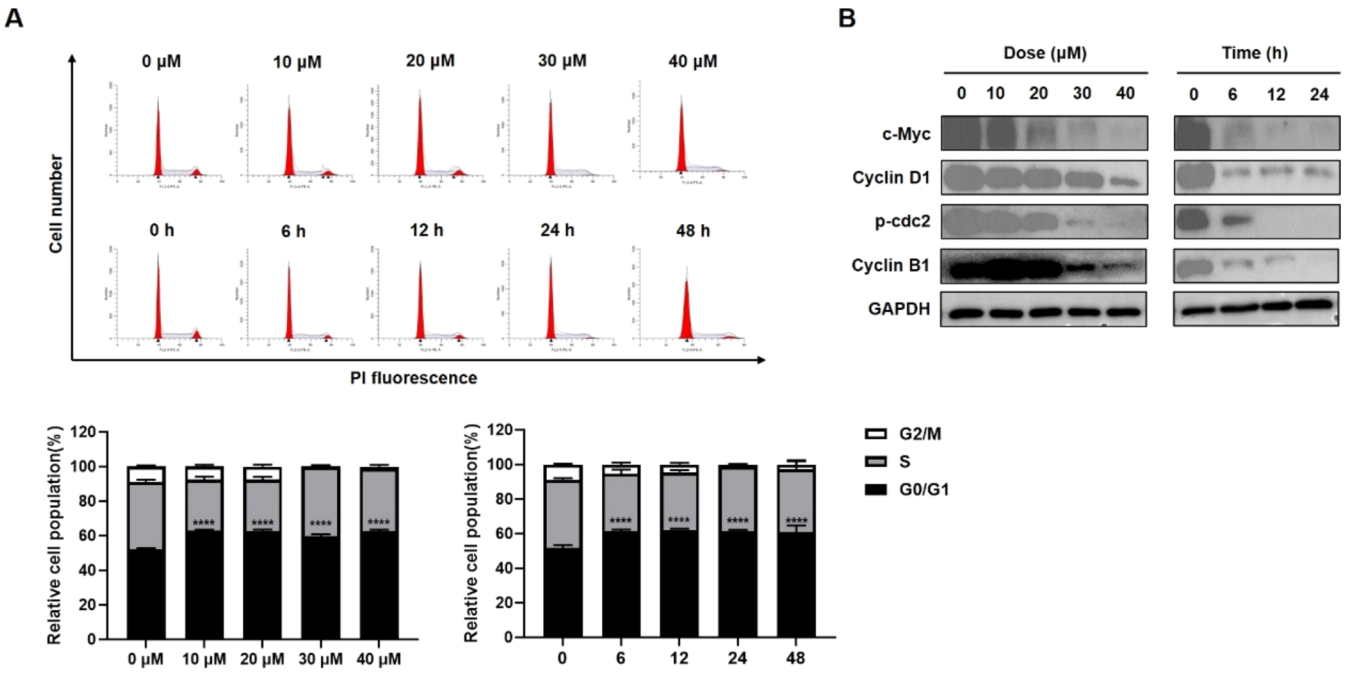


**Figure 2.** SFN-induced cell cycle arrest in the G0/G1 phase in U937 cells. (A) Cells treated with SFN at indicated concentrations or durations; the cell cycle was determined by FACS analysis (upper panel), and bar charts display the statistical analysis results of cell cycle distribution (lower panel). (B) Expression levels of cell-cycle-related proteins analyzed by immunoblotting. Each experiment was repeated three times. ****$P$ < 0.0001.

and the volumes were calculated with the formula (length × width$^2$)/2. The mice were sacrificed at 3 weeks after injection, and the tumors were excised for imaging. Then, the tumors were fixed in paraformaldehyde for immunohistochemical staining. All experimental procedures were approved by the Animal Ethics Committee of the West China Hospital and were performed in accordance with the Guide for the Care and Use of Laboratory Animals.

**2.12. Immunohistochemical Staining.** Paraffin-embedded and sectioned tumor tissues were processed for immunohistochemical staining. In brief, the immunohistochemical staining of caspase-3 (Proteintech, Wuhan, China, 66470-2-Ig), Ki67 (Cell Signaling Technology, MA, #9449), and TRIP13 (Proteintech, Wuhan, China, 67759-1-Ig) was performed using a nonbiotin detection method according to the instructions on the kit (ZSGB-Bio, Beijing, China, PV-8000). Images were observed under a microscope (Leica, Wetzlar, Germany).

**2.13. Statistical Analysis.** All experiments were repeated at least three times, and the data were expressed as means ± standard deviation (SD). Comparisons between groups were evaluated by Student's $t$ test using GraphPad Prism Software (GraphPad Software Inc., CA). The $P$ values were denoted as *$P$ < 0.05, **$P$ < 0.01, ***$P$ < 0.001, and ****$P$ < 0.0001 in all figures.

## 3. RESULTS

**3.1. SFN Inhibited the Proliferation of the Leukemia Cell Line U937.** Sulforaphane (SFN), 1-isothiocyanato-4-methylsulfinyl-butane, is an isothiocyanate found in cruciferous vegetables (Figure 1A), which is one of the most characterized isothiocyanate compounds and has shown anticancer properties. In the present study, we evaluated the effect of SFN on cell proliferation in the leukemia cell line U937. In order to determine the half maximal inhibitory concentration ($IC_{50}$) of SFN on U937 cells, a dose-dependent assay was performed, in which cells were resuspended in fresh medium at 5 × 10$^5$ cells/mL and then treated with SFN at 0−40 $\mu$M for 24 h. The CCK-8 assay was performed to investigate the inhibition ratio of SFN on cell proliferation. The result indicated that SFN inhibited cell proliferation in a dose-dependent manner, and the $IC_{50}$ value of SFN on U937 cells is about 30 $\mu$M (Figure 1B).

**3.2. SFN Induced the Apoptosis of U937 Cells in a Dose- and Time-Dependent Manner.** Apoptosis is a kind of programmed cell death that plays an essential role in controlling cell numbers in many developmental and physiological settings. A dose- and time-dependent assay was performed on U937 cells to evaluate whether SFN could induce the apoptosis of U937 cells. U937 cells were treated with SFN at a series of concentrations (0, 10, 20, 30, and 40 $\mu$M) for 24 h or treated with SFN at 40 $\mu$M for different durations (0, 6, 12, 24, and 48 h), and then the apoptotic cells were detected by flow cytometry with Annexin V-AF647/PI staining. The results showed that when treated with SFN at higher concentrations, more apoptotic cells were detected compared to those of the control or at lower concentrations. On the other hand, more apoptotic cells were detected when treated for a longer time. The percentage of apoptotic cells increased in a dose- and time-dependent manner (Figure 1C). The expression levels of cleaved-PARP and cleaved-caspase-3 are commonly used as markers to assess the occurrence of apoptosis. These cleavage events are indicative of caspase activation and the execution of programmed cell death. Therefore, the expression levels of apoptosis-related proteins (cleaved-PARP and cleaved-caspase-3) were assessed by Western blotting. Consistent with the above results of flow cytometry, these apoptosis-related proteins were significantly increased with an increase in SFN concentrations or treatment times (Figure 1D). All of these results indicated that SFN


https://doi.org/10.1021/acsomega.4c03450
ACS Omega 2024, 9, 26628−26640

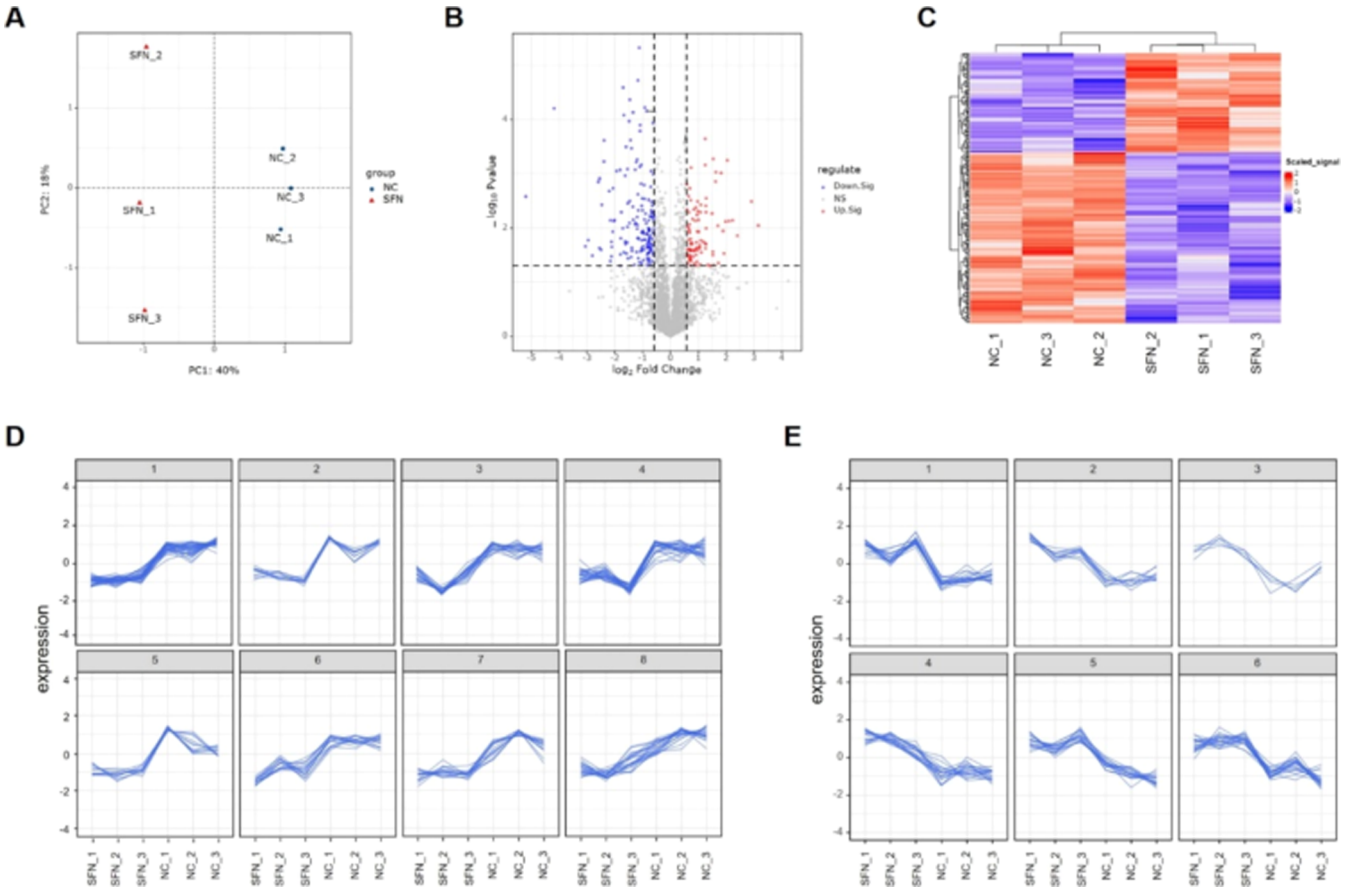


**Figure 3.** SFN treatment changed the protein expression pattern of U937 cells. (A) Principle component analysis (PCA) score plot of proteomic profiling with all identified proteins in control and SFN-treated cells. (B) Volcano plots of differentially expressed proteins in the control and SFN-treated cells. (C) The hierarchically clustered heatmap of the relative abundances of differentially expressed proteins between the control and SFN-treatment groups. (D, E) Clustering analyses of the expression patterns of downregulated and upregulated proteins.

could induce apoptosis of U937 cells in a dose- and time-dependent manner.

**3.3. SFN Induced Cell Cycle Arrest at the G0/G1 Phase in U937 Cells.** As SFN inhibited the proliferation of U937 cells, whether SFN could arrest the cell cycle was also evaluated. U937 cells were treated with SFN at indicated concentrations and durations, and then, the cell cycle was detected with PI staining by flow cytometry. The results showed that the cell cycle was obviously arrested at the G0/G1 phase when treated with SFN at various concentrations and treated for various time durations (Figure 2A). Further, the expression levels of cell-cycle-related proteins were assessed by Western blotting. Consistent with the above results from flow cytometry, the expression levels of c-Myc and cyclin D1, which were the key regulators in the G1-to-S phase transition, were significantly decreased when treated with SFN. Meanwhile, the expression levels of the key regulators of the G2/M transition (p-cdc2 and cyclin B1) were also reduced after SFN treatment (Figure 2B); however, the distribution of the cell cycle in the G2/M phase showed no statistical difference. These results indicated that SFN could mainly arrest the cell cycle at the G0/G1 phase in U937 cells.

**3.4. Proteomic Expression Profiling of SFN-Treated U937 Cells.** In order to further understand protein expression profiling of U937 cells in response to SFN treatment, two groups of U937 cells (control group and SFN-treated group; each group contained three samples) were subjected to a label-free proteomics analysis. A search of the Uniprot database identified a total of 3281 proteins that possessed at least 1 unique peptide with a greater than 95% confidence. The principal component analysis (PCA) showed that, as a result of SFN treatment, the proteomic expression profiling in U937 cells was altered compared with the control group (Figure 3A). These DEPs were further separated with a volcano plot. A total of 238 proteins were identified as DEPs ($\log_2$|fold change| $\geq$ 0.58, $P < 0.05$) from the control U937 cells compared to that with SFN treatment (Supporting Information: Table S1), which included 90 upregulated and 148 downregulated proteins, respectively (Figure 3B). The heatmap analysis illustrated that all experiments were highly reproducible and all DEPs could be distinctly distinguished in the control group from the SFN treatment group. The upregulated and downregulated proteins could be distinctly classified into two groups (Figure 3C). According to the expression pattern, these downregulated DEPs could be mainly grouped into eight distinct clusters. The largest cluster (cluster 1, including 36 proteins) had a consistent overall pattern of downregulation in the SFN treatment group (Figure 3D), and 6 clusters were upregulated steadily in the SFN treatment group compared with the control group (Figure 3E).

**3.5. Bioinformatic Analysis of Differentially Expressed Proteins (DEPs).** The GO enrichment analysis was also performed in up- and downregulated DEPs, respectively, and the most significant terms of enrichment were identified



https://doi.org/10.1021/acsomega.4c03450
ACS Omega 2024, 9, 26628−26640

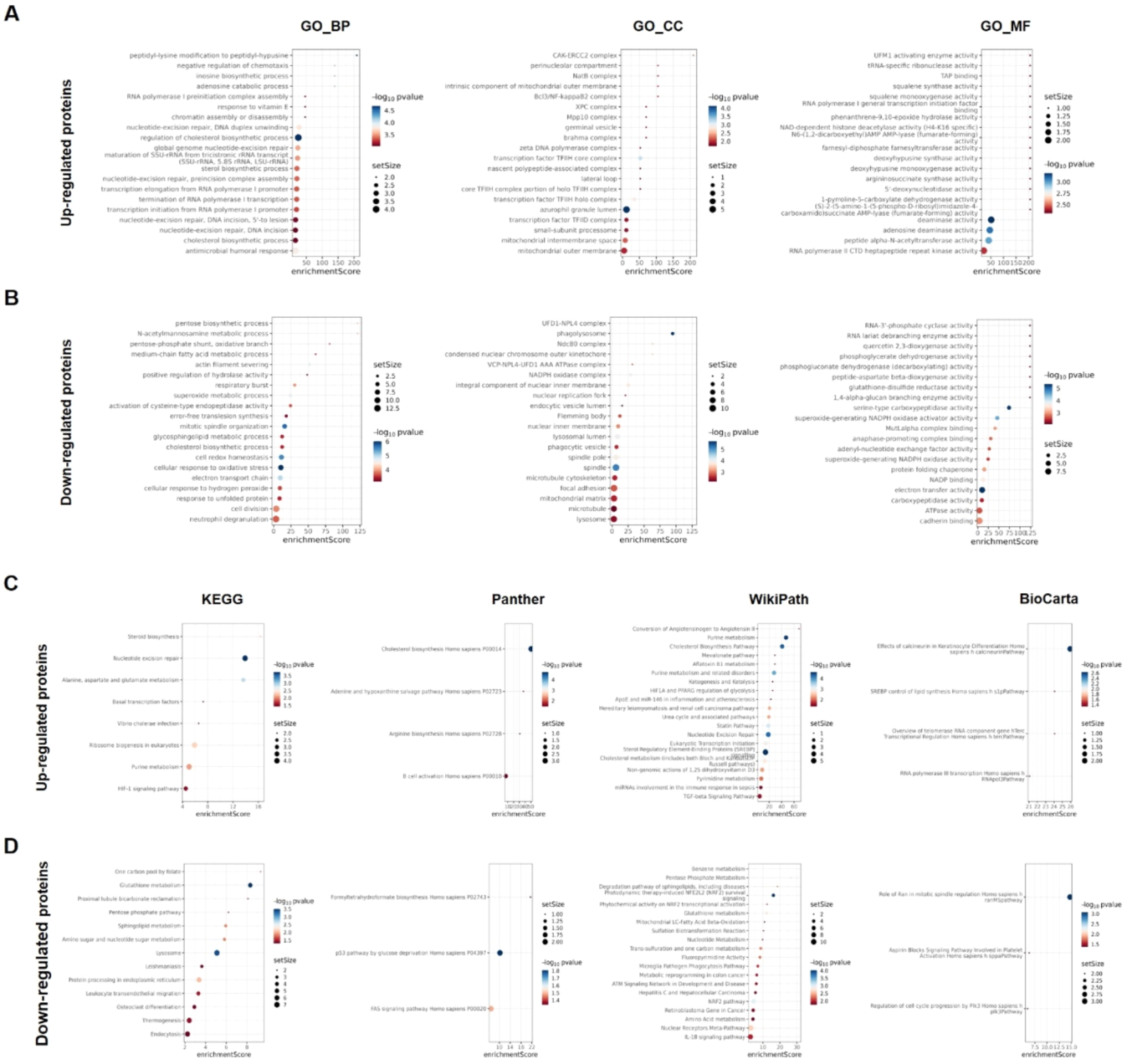


**Figure 4.** Gene ontology (GO) enrichment and pathway analysis of differentially expressed proteins. (A, B) GO function enrichment of the upregulated and downregulated DEPs in biological processes, molecular functions, and cellular components, respectively. (C, D) The pathway enrichment of upregulated and downregulated DEPs analyzed in KEGG, Panther, Wikipath, and BioCarta database, respectively.

($P < 0.05$). For upregulated DEGs, the most significant enrichment was observed in the regulation of the cholesterol biosynthetic process, peptidyl-lysine modification to peptidyl-hypusine, and the adenosine catabolic process of the Biological Process (BP) group, in the azurophil granule lumen, transcription factor TFIIH core complex, and transcription factor TFIIH holo complex of the cellular component (CC) group, and in deaminase activity, adenosine deaminase activity, and peptide $\alpha$-*N*-acetyltransferase activity of the molecular function (MF) group (Figure 4A). For downregulated DEGs, the most significant enrichment was observed in the cellular response to oxidative stress, mitotic spindle organization, and cell redox homeostasis of the BP group, in phagolysosomes, spindle, and UFD1-NPL4 complex of the CC group, and in the electron-transfer activity, serine-type carboxypeptidase activity, and superoxide-generating NADPH oxidase activator activity of the MF group (Figure 4B). These results indicated that the downregulated DEGs were mainly enriched in the processes related to the regulation of cell proliferation and activity, such as mitotic spindle organization and cell redox homeostasis.

Further, we used a series of databases to analyze the signaling pathways involved in DEPs. KEGG is a widely used database that stores a large amount of data about genomes, biological pathways, diseases, chemical substances, and drugs. In the KEGG pathway analysis, nucleotide excision repair and glutathione metabolism were the most significantly enriched among up- and downregulated DEPs, respectively. In addition, the pathway enrichment analysis was performed in several other databases, such as Panther, WikiPath, and BioCarta. The results showed that in the Panther pathway database,


https://doi.org/10.1021/acsomega.4c03450
ACS Omega 2024, 9, 26628−26640

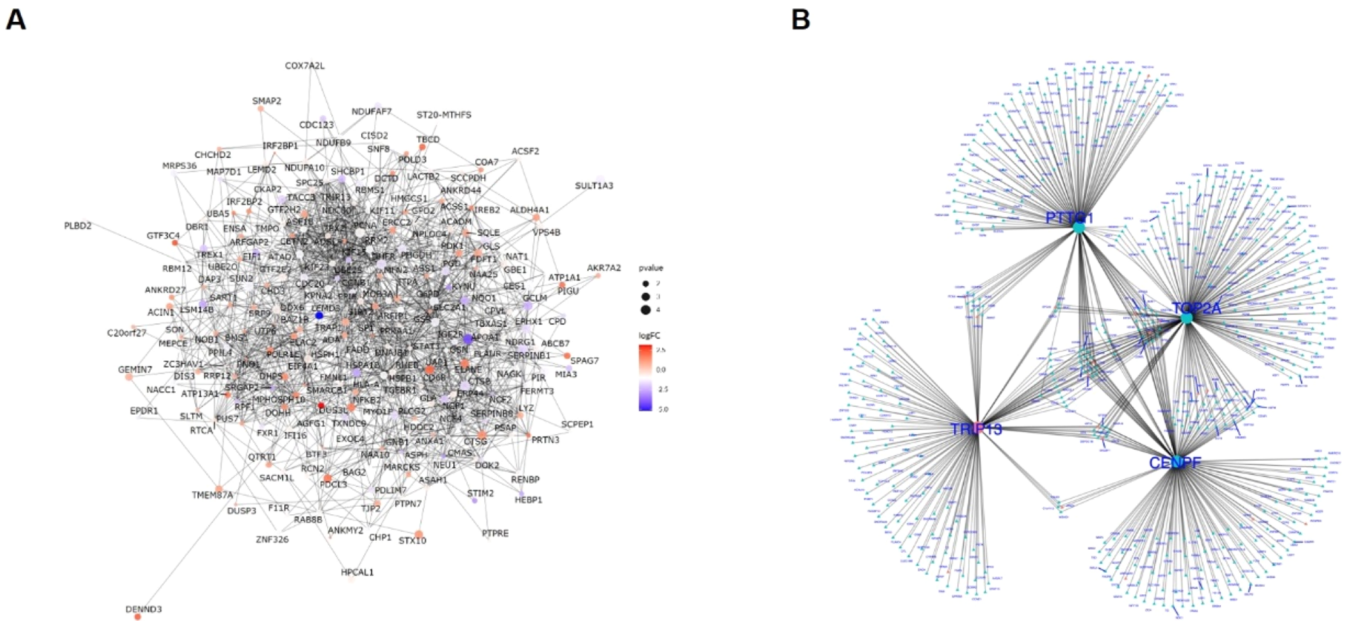


**Figure 5.** Interaction networks of differentially expressed proteins. (A) The protein−protein interaction network of DEPs. The circular nodes represent differentially abundant proteins (red: upregulation; blue: downregulation; circle size: degree of connectivity of the protein, namely, the number of proteins that directly interact with a protein), and the lines represent protein−protein interactions. (B) The key driver analysis predicted driving nodes by using an AML-specific gene regulation network combined with topology analysis. The red node represents the proteins that arise from the differential protein set, and the green node represents the proteins that arise from the background set (i.e., nondifferential proteins but in the regulatory network). The circular nodes represent the top master key driver, and triangles represent nonmaster nodes. The larger node font is the key driver, and the smaller node font is the non-key driver.

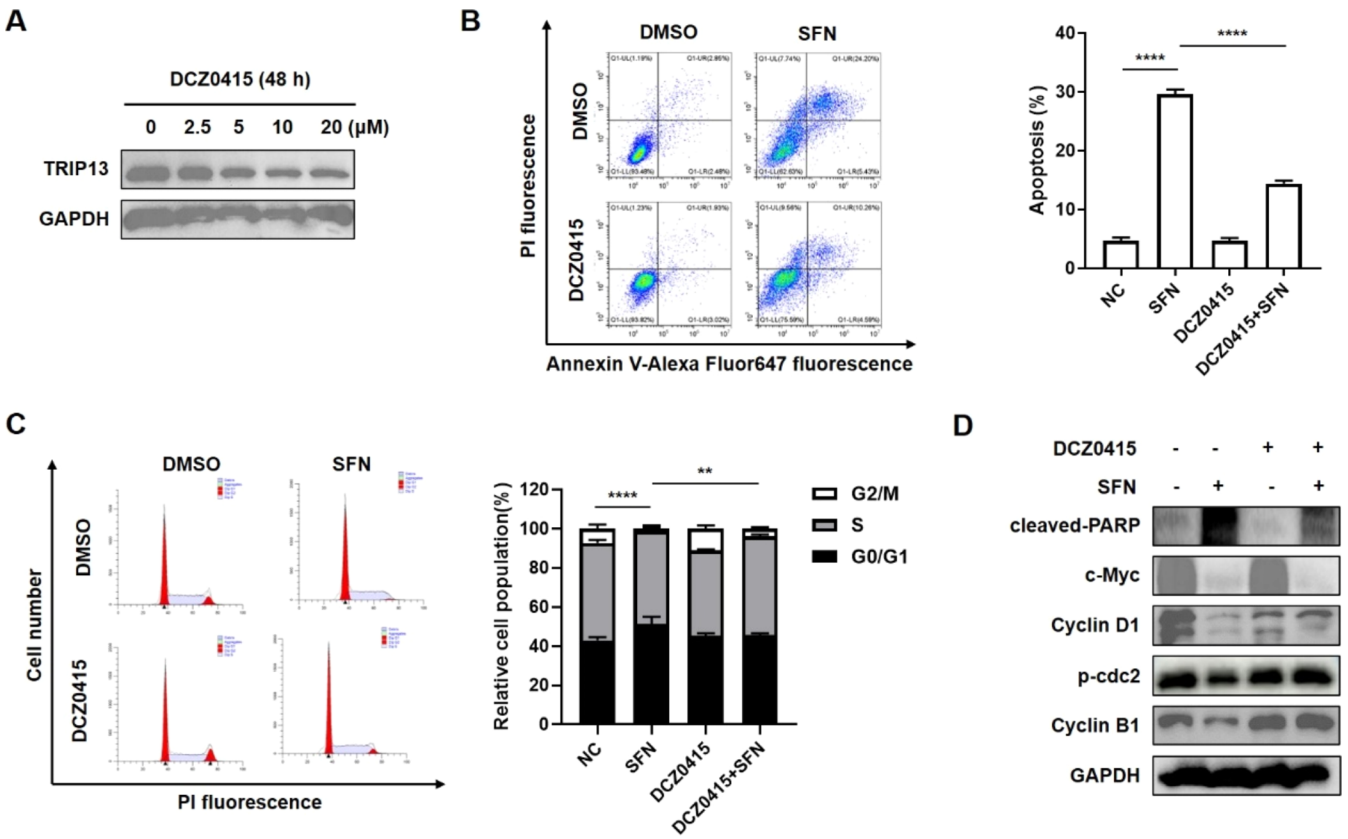


**Figure 6.** TRIP13 was a key protein in SFN-induced leukemia cell apoptosis and cell cycle arrest. (A) Cells were treated with DCZ0415 (the inhibitor of TRIP13) at various concentrations for 48 h, and the inhibitory efficiency was validated by immunoblotting. (B, C) Cells were pretreated with or without DCZ0415 and then treated with SFN. The percentage of apoptotic cells and cell cycle distribution were determined by FACS. (D) Apoptosis and cell-cycle-related proteins were analyzed by immunoblotting. $^{**}P < 0.01$, $^{****}P < 0.0001$.



https://doi.org/10.1021/acsomega.4c03450
ACS Omega 2024, 9, 26628−26640

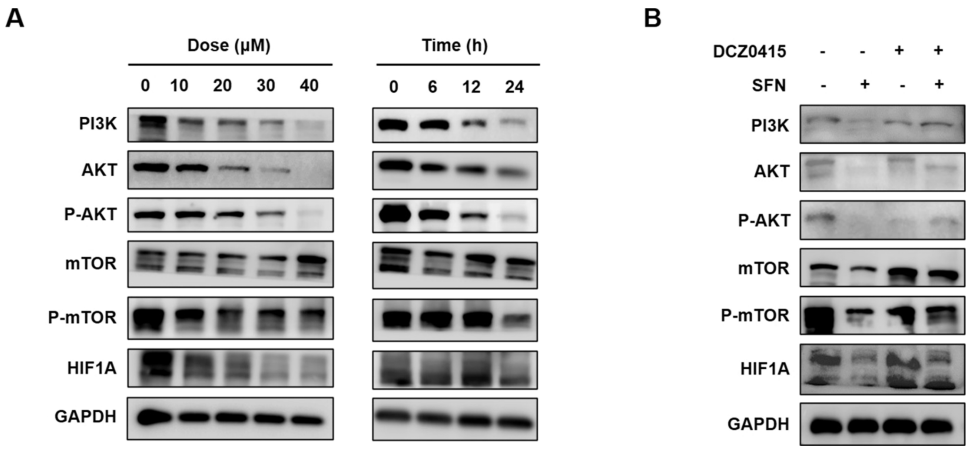


**Figure 7.** TRIP13 played an important role in the SFN-induced cell proliferation inhibition through the mTOR/Akt signaling pathway. (A) Cells were treated with SFN at indicated concentrations for 24 h or treated with 40 $\mu$M SFN for indicated durations, and the key proteins in the mTOR/Akt signaling pathway were detected by immunoblotting. (B) Cells were pretreated with or without DCZ0415 and then treated with SFN. The corresponding proteins were detected by immunoblotting.

cholesterol biosynthesis and the p53 pathway by glucose deprivation were the most significantly enriched in the up- and downregulated DEPs, respectively. The sterol regulatory element-binding protein (SREBP) signaling and photodynamic therapy-induced NFE2L2 (NRF2) survival signaling were the most significantly enriched up- and downregulated DEPs in the WikiPath database. In BioCarta, upregulated DEPs were most significantly enriched in the effects of calcineurin in keratinocyte differentiation pathway, and downregulated DEPs were most significantly enriched in the role of Ran in the mitotic spindle regulation pathway (Figure 4C,D). These results indicated that DEGs were mainly enriched in the signaling pathways related to the regulation of cancer cell proliferation, such as nucleotide excision repair, p53 pathway by glucose deprivation, and the mitotic spindle regulation pathway.

**3.6. Analysis of the Hub Proteins in SFN-Treated U937 Cells.** In order to gain insights into the functions of these DEPs, a protein−protein interaction (PPI) analysis was performed using the STRING online database. After isolated nodes and node pairs were removed, the network included 1344 edges and 219 nodes and a PPI network of DEPs was constructed by Cytoscape. The PPI network shows a large number of closely interacting proteins (Figure 5A). To screen the key factor in SFN-induced growth inhibition of leukemia cells, key driver analysis was performed to predict the driving nodes by using an AML-specific gene regulation network. The result showed that thyroid hormone receptor interactor 13 (TRIP13), which arises from the DEPs, might be the top master key driver in SFN-induced inhibitory effects in U937 cells (Figure 5B).

**3.7. TRIP13 was the Key Regulatory Factor in SFN-Induced Proliferation Inhibition in U937 Cells.** To validate the role of TRIP13 in SFN-induced growth inhibition of leukemia cells, DCZ0415, which is the specific inhibitor of TRIP13, was used in the following study. First, the effective concentration and duration of DCZ0415 in U937 cells were determined. The expression level of TRIP13 was significantly reduced after treatment with 5 $\mu$M DCZ0415 for 48 h (Figure 6A), so this concentration was used in subsequent studies. The role of TRIP13 in SFN-induced apoptosis in U937 cells was detected by flow cytometry and Western blotting. The results showed that pretreatment with DCZ0415 could significantly attenuate SFN-induced cell apoptosis (Figure 6B). In addition, inhibition of TRIP13 could also significantly attenuate SFN-induced cell cycle arrest at the G0/G1 phase (Figure 6C). Consistently, compared to the SFN group, the expression levels of apoptosis and cell-cycle-related proteins were increased to a certain extent in the DCZ0415-pretreated group (Figure 6D). These results validated that TRIP13 was a key factor in SFN-induced apoptosis and cell cycle arrest in U937 cells.

**3.8. TRIP13 Plays a Key Role in SFN-Induced Proliferation Inhibition through the PI3K/Akt/mTOR Signaling Pathway.** The PI3K/Akt/mTOR signaling pathway plays a critical role in the regulation of cell growth, proliferation, survival, and metabolism. In leukemia, aberrations in this pathway are often observed, contributing to the development and progression of the disease. Therefore, targeting the PI3K/Akt/mTOR pathway holds promise as a therapeutic strategy in leukemia. Recently, some evidence suggested that TRIP13 can modulate the activity of the PI3K/Akt/mTOR signaling pathway so as to participate in cancer progression, such as in lung cancer,[14,15] breast cancer,[16] and hepatocellular carcinoma.[17] However, the relationship between TRIP13 and PI3K/Akt/mTOR in leukemia still needs to be fully understood. In order to investigate the molecular mechanism of TRIP13 in affecting the SFN-induced growth inhibition of leukemia cells, the key proteins in the PI3K/Akt/mTOR signaling pathway were detected by immunoblotting. After treatment with SFN, the expression levels of PI3 kinase, phospho-Akt, phospho-mTOR, and the downstream molecule HIF-1$\alpha$ were significantly reduced in U937 cells (Figure 7A). When the U937 cells were pretreated with DCZ0415, the reduction expression levels of these key proteins in the PI3K/Akt/mTOR signaling pathway, which was caused by SFN, could be obviously attenuated (Figure 7B). These results indicated that SFN could inhibit the activity of the PI3K/Akt/mTOR signaling pathway, and TRIP13 plays an important role in the process.

**3.9. TRIP13 was the Key Regulatory Factor in SFN-Induced Proliferation Inhibition In Vivo.** To further validate the role of TRIP13 in SFN-induced growth inhibition in vivo, the xenograft model mice were divided into four


https://doi.org/10.1021/acsomega.4c03450
ACS Omega 2024, 9, 26628−26640

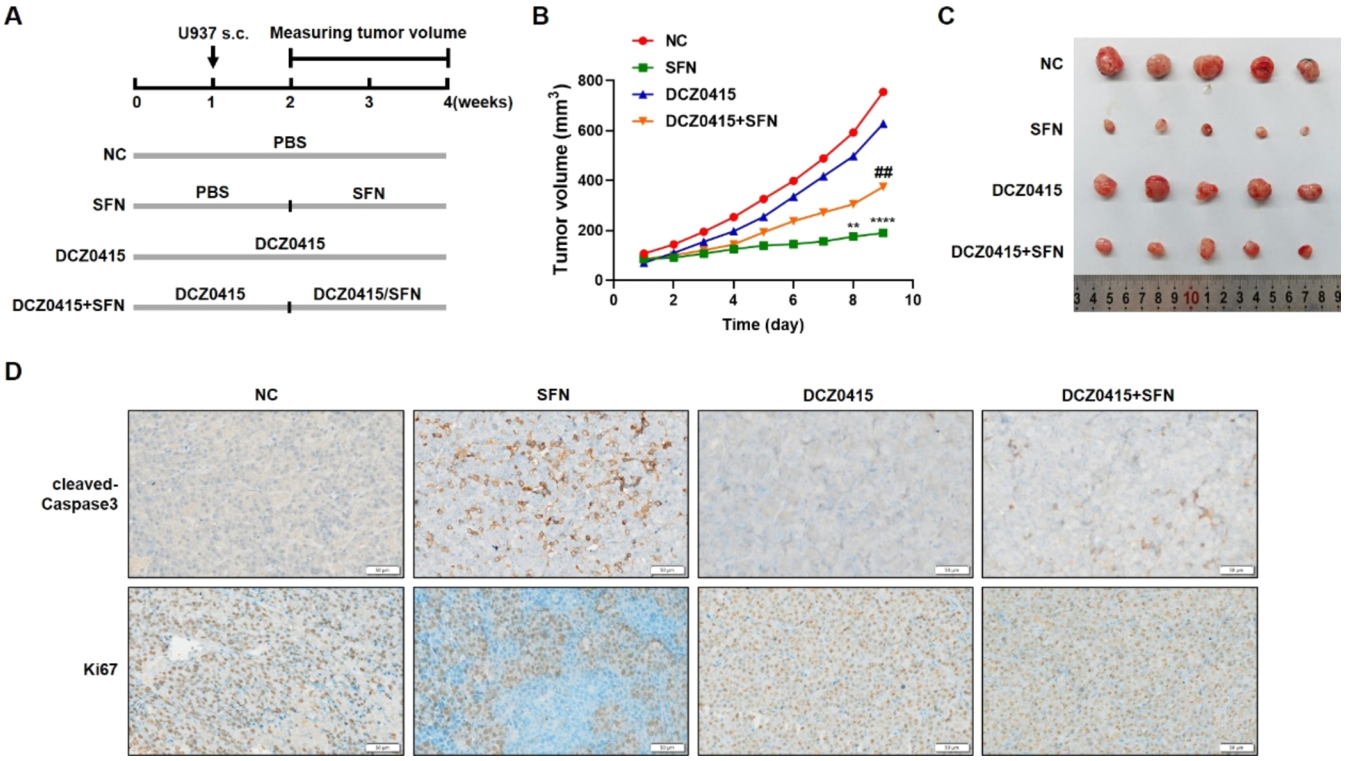


**Figure 8.** TRIP13 is a key protein in SFN-induced leukemia cell growth inhibition in vivo. (A) Schematic of the experimental design to evaluate the effect of SFN and TRIP13 on leukemia cell growth in vivo. (B) Tumor volumes were measured at the indicated days and tumor growth curves were drawn. The data points represent the mean value of tumor volumes in each group. (C) The image of subcutaneous tumors from each group. (D) The representative immunohistochemical images of the expression of apoptosis and proliferation-related proteins in each group. *: compared with the NC group; #: compared with the SFN group. $^{**}P < 0.01$, $^{****}P < 0.0001$, and $^{\#\#}P < 0.01$.

groups: control group, SFN group, DCZ0415 group, and DCZ0415 + SFN group (Figure 8A). Compared to the control group, suppressed tumor growth was apparent 8 days after initiating SFN treatment. When DCZ0415 was previously injected 1 week before the xenograft inoculation, tumor growth was promoted 9 days after SFN treatment compared with the SFN group (Figure 8B). Consistently, the tumor volume in the SFN group was significantly inhibited, and the inhibitory effect could be obviously attenuated under the pretreatment with DCZ0415 (Figure 8C). Further, to analyze the expression of apoptosis- and proliferation-related proteins, the tumor tissue was excised, embedded, and sectioned for immunohistochemical staining. The results revealed that, compared with the NC group, the tumor tissue of SFN-treated mice had increased immunoreactivity for cleaved-caspase-3, an indicator of apoptosis. Furthermore, treatment with SFN resulted in an obvious decrease in the expression level of Ki67, an indicator of proliferation. However, when pretreated with DCZ0415, the effect of SFN on inducing apoptosis and inhibiting proliferation was significantly diminished (Figure 8D). Taken together, these findings indicate that SFN significantly inhibited the growth of U937 cells in vivo, and these effects were associated with the expression level of TRIP13.

## 4. DISCUSSION

The growth inhibition effect of SFN was recently demonstrated in leukemia cell lines via various mechanisms. On the one hand, SFN could induce apoptosis in leukemia cells through oxidative damage,[9] Fas- and mitochondria-dependent pathways,[12] an increase in the expression of p53,[18,19] and other mechanisms.[6,20] On the other hand, SFN could inhibit cell proliferation via cell cycle arrest. SFN arrested cell cycle progression in the G1 phase through a decrease in the protein expression of cyclin D3 in Jurkat T-leukemia cells.[18,19] In the present study, the cell cycle was significantly arrested at the G0/G1 phase with SFN treatment in U937 cells. Consistently, the expression levels of cell cycle regulatory proteins c-Myc and Cyclin D1 were obviously decreased. C-Myc is a transcription factor that is involved in cell cycle entry and progression from the G0/G1 to the S phase. It also activates genes involved in DNA replication and cell growth, contributing to cell cycle progression.[21] Cyclin D1 is involved in the G1 phase of the cell cycle. It forms complexes with cyclin-dependent kinases (CDK4/6), promoting the progression of the cell cycle from the G1 to the S phase by phosphorylating and inactivating the retinoblastoma protein (Rb).[22] These results indicate that SFN mainly arrested the cell cycle at the G0/G1 phase in U937 cells. Previous studies reported that SFN also caused G2/M phase arrest in Jurkat T-leukemia cells in a time- and dose-dependent manner[23] and G2/M phase arrest in ALL cell lines via a p53-independent upregulation of p21(CIP1/WAF1) and inhibition of the Cdc2/Cyclin B1 complex.[20] In our study, the expression levels of p-cdc2 and cyclin B1 were also reduced after SFN treatment. Cdc2, also known as CDK1, is a key regulator of the G2/M transition. It forms complexes with cyclin B to drive entry into mitosis. Phosphorylation of cdc2 (p-cdc2) leads to its activation, and the presence of phospho-cdc2 indicates a transition from the G2 to the M phase of the cell cycle.[24] Cyclin B1 plays a crucial role, particularly in the transition from the G2 phase to the M phase (mitosis). It is one of the key regulators of cell cycle progression and is involved in the


https://doi.org/10.1021/acsomega.4c03450
ACS Omega 2024, 9, 26628−26640

initiation and progression of mitosis.[25] However, the results of flow cytometry showed that the distribution of cells in the G2/M phase was not statistically different. This may be because p-cdc2 and cyclin B1 also participated in regulating many other cellular events, such as mitochondrial bioenergetics, cancer progression, and drug resistance.[26,27]

In the present study, GO-BP enrichment analysis revealed that the top three significantly enriched terms of these downregulated DEGs were cellular response to oxidative stress, mitotic spindle organization, and cell redox homeostasis. Oxidative stress could activate intrinsic apoptotic pathways. It could also elevate reactive oxygen species (ROS) levels and disrupt redox homeostasis in cancer cells. This ultimately leads to damage to tumor cells with ROS levels exceeding a certain threshold.[28] Consistently, in the GO-MF enrichment, electron-transfer activity, serine-type carboxypeptidase activity, and superoxide-generating NADPH oxidase activator activity were the top three enriched terms. These results indicated that SFN may induce cell apoptosis mainly by regulating oxidation−reduction homeostasis. In addition, the results of the GO-CC enrichment analysis were significantly enriched in phagolysosomes, spindles, and the UFD1-NPL4 complex; meanwhile, mitotic spindle organization was also enriched in GO-BP analysis. These results suggested that SFN may inhibit cell proliferation by regulating the cell cycle, which is consistent with the results of flow cytometry.

In the pathway analysis, the top three significantly enriched pathways of these downregulated DEGs were in glutathione metabolism, lysosome, and protein processing in the endoplasmic reticulum by KEGG analysis. Interestingly, the phagolysosome was the most significantly enriched term in the GO-CC enrichment analysis. It indicated that autophagy may also be involved in SFN-induced cell growth inhibition. This is consistent with a previous report that SFN inhibited cell growth and induced autophagy by the inhibition of HDAC6-mediated PTEN activation in triple-negative breast cancer cells.[29] In the Panther pathway analysis, the p53 pathway by glucose deprivation, the FAS signaling pathway, and formyltetrahydroformate biosynthesis were the top three significantly enriched pathways of downregulated DEPs. Glucose deprivation could enhance tumor necrosis factor (TNF)-related apoptosis-inducing ligand (TRAIL)-induced apoptosis by integrating the activating transcription factor 4 (ATF4)-C/EBP-homologous protein (CHOP)-p53 upregulated modulator of apoptosis (PUMA) axis, consequently amplifying the Bid-Bax-associated mitochondria-dependent pathway.[30] The FAS signaling pathway plays an important role in cell extrinsic apoptosis.[31] This result indicated that SFN may induce cell growth inhibition by activating both the intrinsic mitochondrial pathway and the extrinsic death receptor pathway. In addition, the WikiPath database analysis showed that the downregulated DEPs caused by SFN treatment were mainly enriched in the NRF2 pathway. NRF2 is a crucial transcription factor that helps maintain redox homeostasis and it is a potential target for cancer treatment.[32] Recently, the molecular biology and therapeutic potential of NRF2 in leukemia was reported. High levels of *NFE2L2*, which encoded NRF2, may be a predictive biomarker of poor treatment response in T-cell acute lymphoblastic leukemia (T-ALL) patients.[33] NRF2 could also protect leukemic cells from the effects of chemotherapeutic drugs. NRF2 knockdown enhanced the sensitivity of AML cells to the ferroptosis inducers.[34] Targeted silencing of NRF2 by rituximab-conjugated nanoparticles increases the sensitivity of chronic lymphoblastic leukemia cells to cyclophosphamide.[35] The results of the WikiPath analysis suggested that SFN may inhibit cell growth by suppressing the activity of the NRF2 pathway, which was consistent with the above studies. In the BioCarta pathway database analysis, the downregulated DEPs caused by SFN treatment were mainly enriched in the role of Ran in mitotic spindle regulation and regulation of cell cycle progression by PIk3, which was consistent with the results of flow cytometry analysis and immunoblotting. These results of pathway analysis indicated that the DEGs mainly enriched in regulating cancer cell proliferation, such as lysosome, p53 pathway, FAS signaling pathway, NRF2 pathway, and the cell-cycle-related pathway.

Performing the key driver analysis in a specific disease database could help screen key factors more efficiently.[36] In the present study, in order to screen the key factor in leukemia cell response to SFN treatment, key driver analysis was performed in the AML-specific gene regulation network. The result showed that TRIP13, which arises from DEPs, might be the top master key driver. TRIP13 is a critical mitosis regulator and plays a key role in regulating mitotic processes and the cell cycle. In colorectal cancer (CRC) cells, TRIP13 knockdown resulted in cell cycle arrest in the G1 phase.[37] Treatment with the TRIP13 inhibitor DCZ0415 resulted in decreased CRC cell proliferation and induced cell cycle arrest in the G2-M phase.[38] Another research reported that DCZ0415 could induce a G0/G1 phase arrest of CRC cells.[39] In lung cancer cells, TRIP13 knockdown increased apoptosis and inhibited proliferation by inducing cell cycle arrest of H1299 cells in the S phase.[40] In the present study, treatment with SFN could induce cell cycle arrest in the G0/G1 phase by regulating TRIP13, and inhibition of TRIP13 expression by pretreatment with inhibitor DCZ0415 could significantly attenuate SFN-induced cell cycle arrest in the G0/G1 phase. The result indicated that TRIP13 was the key factor in SFN-induced cell cycle arrest in U937 cells.

Recent studies suggested that TRIP13 functions as an oncogene in multiple cancers. Amplification of TRIP13 has been observed in various human cancers,[14,41−44] and it is implicated in several aspects of malignant transformation, including cancer cell apoptosis,[45] cell cycle,[44] proliferation,[41,42] invasion,[46] and drug resistance.[47,48] TRIP13 also plays an important role in leukemia. The TRIP13 mRNA levels of $CD19^+$ B cells were 4-fold higher in chronic lymphocytic leukemia patients than in healthy persons, and the loss of TRIP13 inhibits cell proliferation and survival in human chronic lymphocytic leukemia.[49] TRIP13 could also modulate protein deubiquitination and accelerate tumor development and progression of B cell malignancies.[50] Therefore, TRIP13 was considered to be a novel therapeutic target, and there have been some genetic and drug studies targeting TRIP13. TRIP13 depletion in liver cancer induces a lipogenic response contributing to Plin2-dependent mitotic cell death.[51] Some ceRNAs have been reported to be involved in regulating the expression of TRIP13, thereby playing a role in tumor progression.[37,39,52] Recently, some small-molecule inhibitors, which specifically target TRIP13, have been used to treat tumors. The cantharidin derivatives DCZ5417 and DCZ5418 were designed and synthesized as TRIP13 inhibitors, which could suppress multiple myeloma progression in vitro and in vivo.[53,54] DCZ0415 is the most commonly used inhibitor of TRIP13. DCZ0415 could also suppress multiple myeloma


https://doi.org/10.1021/acsomega.4c03450
ACS Omega 2024, 9, 26628−26640

progression[55] and inhibit EMT and metastasis by the inactivation of the FGFR4/STAT3 axis and the Wnt/β-catenin pathway in colorectal cancer.[38] Some studies suggested that TRIP13 is related to tumor resistance. TRIP13 could alleviate osimertinib-triggered paraptosis in glioblastoma cells,[47] and TRIP13 overexpression promotes gefitinib resistance in nonsmall-cell lung cancer by regulating autophagy and phosphorylation of the epidermal growth factor receptor (EGFR) signaling pathway.[48] However, some researchers proposed that TRIP13 is related to tumor chemotherapy sensitization. Head and neck tumors expressing high TRIP13 do not respond to radiation but are sensitive to cetuximab or cetuximab combined with radiation.[56] In the present study, the expression level of TRIP13 was to some extent decreased after treatment with SFN. However, inhibition of TRIP13 by the specific inhibitor DCZ0415 could significantly attenuate SFN-induced U937 cell proliferation inhibition in vitro and in vivo through the PI3K/Akt/mTOR pathway, which plays a key role in promoting survival of leukemia cells.[57] The result indicated that TRIP13 plays an important role in the sensitivity of the leukemia cell response to sulforaphane treatment. However, the mechanism of downregulation of TRIP13 by treatment with SFN and the molecular mechanism of SFN-mediated cell growth inhibition are complex and still unclear. We will conduct further research on this issue in the future. In summary, TRIP13 is the key factor in SFN-induced cell growth suppression, and it may be a potential treatment target in leukemia treatment.

## ■ ASSOCIATED CONTENT

### Data Availability Statement

The data is available throughout the manuscript and Supporting Files.

### Supporting Information

The Supporting Information is available free of charge at https://pubs.acs.org/doi/10.1021/acsomega.4c03450.

Details of identified differentially expressed proteins from the control cells compared to SFN treatment in Figures 3−5 (XLSX)

## ■ AUTHOR INFORMATION


### Corresponding Authors

**Yan Li** − *Department of General Surgery, The 77th Army Hospital, Leshan 614000 Sichuan, China*; Email: liyan.free@163.com

**Jing Li** − *Department of Pharmacological Research Lab, The Beibei Affiliated Hospital of Chongqing Medical University, The Ninth People's Hospital of Chongqing, Chongqing 400799, China*; orcid.org/0009-0006-7506-0982; Email: jingli150324@126.com

### Authors

**Lei Liu** − *Medical Research Center, The Third People's Hospital of Chengdu (Affiliated Hospital of Southwest Jiaotong University), College of Medicine, Southwest Jiaotong University, Chengdu 610031 Sichuan, China*; orcid.org/0000-0002-8691-4465

**Baixue Liao** − *College of Medicine, Southwest Jiaotong University, Chengdu 610031 Sichuan, China*

**Ruiling Fan** − *School of Pharmacy, North Sichuan Medical College, Nanchong 637000 Sichuan, China*

**Yanxia Liu** − *College of Pharmacy, Third Military Medical University (Army Medical University), Chongqing 400038, China*

**Aoshuang Li** − *College of Medicine, Southwest Jiaotong University, Chengdu 610031 Sichuan, China*

**Lüye Liu** − *Medical Research Center, The Third People's Hospital of Chengdu (Affiliated Hospital of Southwest Jiaotong University), College of Medicine, Southwest Jiaotong University, Chengdu 610031 Sichuan, China*

Complete contact information is available at: https://pubs.acs.org/10.1021/acsomega.4c03450


### Author Contributions

[▽]L.L. and B.L. contributed equally to this work.


### Funding

This work was supported by grants from The Chongqing Natural Science Foundation (cstc2021jcyj-msxmX0175) and The Third People's Hospital of Chengdu Scientific Research Project (2023PI19).


### Notes

The authors declare no competing financial interest.

## ■ REFERENCES


(1) Li, S.; Khoi, P. N.; Yin, H.; Sah, D. K.; Kim, N. H.; Lian, S.; Jung, Y. D. Sulforaphane Suppresses the Nicotine-Induced Expression of the Matrix Metalloproteinase-9 via Inhibiting ROS-Mediated AP-1 and NF-kappaB Signaling in Human Gastric Cancer Cells. *Int. J. Mol. Sci.* **2022**, *23* (9), No. 5172, DOI: 10.3390/ijms23095172.

(2) Xie, H.; Rutz, J.; Maxeiner, S.; Grein, T.; Thomas, A.; Juengel, E.; Chun, F. K.; Cinatl, J.; Haferkamp, A.; Tsaur, I.; Blaheta, R. A. Plant-Derived Sulforaphane Suppresses Growth and Proliferation of Drug-Sensitive and Drug-Resistant Bladder Cancer Cell Lines In Vitro. *Cancers* **2022**, *14* (19), No. 4682, DOI: 10.3390/cancers14194682.

(3) Hung, C.-M.; Tsai, T. H.; Lee, K. T.; Hsu, Y. C. Sulforaphane-Induced Cell Mitotic Delay and Inhibited Cell Proliferation via Regulating CDK5R1 Upregulation in Breast Cancer Cell Lines. *Biomedicines* **2023**, *11* (4), No. 996, DOI: 10.3390/biomedicines11040996.

(4) Chen, Y.; Tang, L.; Ye, X.; Chen, Y.; Shan, E.; Han, H.; Zhong, C. Regulation of ZO-1 on beta-catenin mediates sulforaphane suppressed colorectal cancer stem cell properties in colorectal cancer. *Food Funct.* **2022**, *13* (23), 12363−12370.

(5) Tuttis, K.; Machado, A. R. T.; Santos, P.; Antunes, L. M. G. Sulforaphane Combined with Vitamin D Induces Cytotoxicity Mediated by Oxidative Stress, DNA Damage, Autophagy, and JNK/MAPK Pathway Modulation in Human Prostate Tumor Cells. *Nutrients* **2023**, *15* (12), No. 2742, DOI: 10.3390/nu15122742.

(6) Koolivand, M.; Ansari, M.; Moein, S.; Afsa, M.; Malekzadeh, K. The Inhibitory Effect of Sulforaphane on The Proliferation of Acute Myeloid Leukemia Cell Lines through Controlling miR-181a. *Cell J.* **2022**, *24* (1), 44−50, DOI: 10.22074/cellj.2022.7508.

(7) Núñez-Sánchez, M. Á.; Martinez-Sanchez, M. A.; Verdejo-Sanchez, M.; Garcia-Ibanez, P.; Oliva Bolarin, A.; Ramos-Molina, B.; Moreno, D. A.; Ruiz-Alcaraz, A. J. Anti-Leukemic Activity of Brassica-Derived Bioactive Compounds in HL-60 Myeloid Leukemia Cells. *Int. J. Mol. Sci.* **2022**, *23* (21), No. 13400, DOI: 10.3390/ijms232113400.

(8) Wang, F.; Huang, X.; Sun, Y.; Li, Z.; Sun, R.; Zhao, T.; Wang, M.; Yan, C.; Liu, P. Sulforaphane regulates the proliferation of leukemia stem-like cells via Sonic Hedgehog signaling pathway. *Eur. J. Pharmacol.* **2022**, *919*, No. 174824.

(9) Prada-Arismendy, J.; Arroyave, J. C.; Rothlisberger, S. Molecular biomarkers in acute myeloid leukemia. *Blood Rev.* **2017**, *31* (1), 63−76.

(10) Shang, H. S.; Shih, Y. L.; Lee, C. H.; Hsueh, S. C.; Liu, J. Y.; Liao, N. C.; Chen, Y. L.; Huang, Y. P.; Lu, H. F.; Chung, J. G.

Sulforaphane-induced apoptosis in human leukemia HL-60 cells through extrinsic and intrinsic signal pathways and altering associated genes expression assayed by cDNA microarray. *Environ. Toxicol* **2017**, *32* (1), 311−328.
(11) Greco, G.; Schnekenburger, M.; Catanzaro, E.; Turrini, E.; Ferrini, F.; Sestili, P.; Diederich, M.; Fimognari, C. Discovery of Sulforaphane as an Inducer of Ferroptosis in U-937 Leukemia Cells: Expanding Its Anticancer Potential. *Cancers* **2022**, *14* (1), No. 76, DOI: 10.3390/cancers14010076.
(12) Koolivand, M.; Ansari, M.; Piroozian, F.; Moein, S.; MalekZadeh, K. Alleviating the progression of acute myeloid leukemia (AML) by sulforaphane through controlling miR-155 levels. *Mol. Biol. Rep.* **2018**, *45* (6), 2491−2499.
(13) Lu, S.; Qian, J.; Guo, M.; Gu, C.; Yang, Y. Insights into a Crucial Role of TRIP13 in Human Cancer. *Comput. Struct. Biotechnol. J.* **2019**, *17*, 854−861.
(14) Li, W.; Zhang, G.; Li, X.; Wang, X.; Li, Q.; Hong, L.; Shen, Y.; Zhao, C.; Gong, X.; Chen, Y.; Zhou, J. Thyroid hormone receptor interactor 13 (TRIP13) overexpression associated with tumor progression and poor prognosis in lung adenocarcinoma. *Biochem. Biophys. Res. Commun.* **2018**, *499* (3), 416−424.
(15) Cai, W.; Ni, W.; Jin, Y.; Li, Y. TRIP13 promotes lung cancer cell growth and metastasis through AKT/mTORC1/c-Myc signaling. *Cancer Biomarkers* **2021**, *30* (2), 237−248.
(16) Lan, J.; Huang, J.; Tao, X.; Gao, Y.; Zhang, L.; Huang, W.; Luo, J.; Liu, C.; Deng, Y.; Liu, L.; Liu, X. Evaluation of the TRIP13 level in breast cancer and insights into potential molecular pathways. *J. Cell Mol. Med.* **2022**, *26* (9), 2673−2685.
(17) Zhu, M. X.; Wei, C. Y.; Zhang, P. F.; Gao, D. M.; Chen, J.; Zhao, Y.; Dong, S. S.; Liu, B. B. Elevated TRIP13 drives the AKT/mTOR pathway to induce the progression of hepatocellular carcinoma via interacting with ACTN4. *J. Exp. Clin. Cancer Res.* **2019**, *38* (1), No. 409, DOI: 10.1186/s13046-019-1401-y.
(18) Fimognari, C.; Nusse, M.; Berti, F.; Iori, R.; Cantelli-Forti, G.; Hrelia, P. Sulforaphane modulates cell cycle and apoptosis in transformed and non-transformed human T lymphocytes. *Ann. N. Y. Acad. Sci.* **2003**, *1010*, 393−398.
(19) Fimognari, C.; Nusse, M.; Berti, F.; Iori, R.; Cantelli-Forti, G.; Hrelia, P. Cyclin D3 and p53 mediate sulforaphane-induced cell cycle delay and apoptosis in non-transformed human T lymphocytes. *Cell. Mol. Life Sci.* **2002**, *59* (11), 2004−2012.
(20) Suppipat, K.; Park, C. S.; Shen, Y.; Zhu, X.; Lacorazza, H. D. Sulforaphane induces cell cycle arrest and apoptosis in acute lymphoblastic leukemia cells. *PLoS One* **2012**, *7* (12), No. e51251.
(21) Dang, C. V. c-Myc target genes involved in cell growth, apoptosis, and metabolism. *Mol. Cell. Biol.* **1999**, *19* (1), 1−11.
(22) Malumbres, M.; Barbacid, M. Mammalian cyclin-dependent kinases. *Trends Biochem. Sci.* **2005**, *30* (11), 630−641.
(23) Fimognari, C.; Nusse, M.; Cesari, R.; Iori, R.; Cantelli-Forti, G.; Hrelia, P. Growth inhibition, cell-cycle arrest and apoptosis in human T-cell leukemia by the isothiocyanate sulforaphane. *Carcinogenesis* **2002**, *23* (4), 581−586.
(24) Crncec, A.; Hochegger, H. Triggering mitosis. *FEBS Lett.* **2019**, *593* (20), 2868−2888.
(25) Miyazaki, T.; Arai, S. Two distinct controls of mitotic cdk1/cyclin B1 activity requisite for cell growth prior to cell division. *Cell Cycle* **2007**, *6* (12), 1419−1425.
(26) Massacci, G.; Perfetto, L.; Sacco, F. The Cyclin-dependent kinase 1: more than a cell cycle regulator. *Br. J. Cancer* **2023**, *129* (11), 1707−1716.
(27) Xie, B.; Wang, S.; Jiang, N.; Li, J. J. Cyclin B1/CDK1-regulated mitochondrial bioenergetics in cell cycle progression and tumor resistance. *Cancer Lett.* **2019**, *443*, 56−66.
(28) Ren, Y.; Wang, R.; Weng, S.; Xu, H.; Zhang, Y.; Chen, S.; Liu, S.; Ba, Y.; Zhou, Z.; Luo, P.; Cheng, Q.; Dang, Q.; Liu, Z.; Han, X. Multifaceted role of redox pattern in the tumor immune microenvironment regarding autophagy and apoptosis. *Mol. Cancer* **2023**, *22* (1), No. 130, DOI: 10.1186/s12943-023-01831-w.
(29) Yang, F.; Wang, F.; Liu, Y.; Wang, S.; Li, X.; Huang, Y.; Xia, Y.; Cao, C. Sulforaphane induces autophagy by inhibition of HDAC6-mediated PTEN activation in triple negative breast cancer cells. *Life Sci.* **2018**, *213*, 149−157.
(30) Kalimuthu, K.; Kim, J. H.; Park, Y. S.; Luo, X.; Zhang, L.; Ku, J. L.; Choudry, M. H. A.; Lee, Y. J. Glucose deprivation-induced endoplasmic reticulum stress response plays a pivotal role in enhancement of TRAIL cytotoxicity. *J. Cell Physiol.* **2021**, *236* (9), 6666−6677.
(31) Green, D. R.; Llambi, F. Cell Death Signaling. *Cold Spring Harbor Perspect. Biol.* **2015**, *7* (12), No. a006080, DOI: 10.1101/cshperspect.a006080.
(32) Sivinski, J.; Zhang, D. D.; Chapman, E. Targeting NRF2 to treat cancer. *Semin. Cancer Biol.* **2021**, *76*, 61−73.
(33) Villa-Morales, M.; Perez-Gomez, L.; Perez-Gomez, E.; Lopez-Nieva, P.; Fernandez-Navarro, P.; Santos, J. Identification of NRF2 Activation as a Prognostic Biomarker in T-Cell Acute Lymphoblastic Leukaemia. *Int. J. Mol. Sci.* **2023**, *24* (12), No. 10350, DOI: 10.3390/ijms241210350.
(34) Liu, X.; Zhong, S.; Qiu, K.; Chen, X.; Wu, W.; Zheng, J.; Liu, Y.; Wu, H.; Fan, S.; Nie, D.; Wang, X.; Yu, Z.; Liao, Z.; Zhong, M.; Li, Y.; Zeng, C. Targeting NRF2 uncovered an intrinsic susceptibility of acute myeloid leukemia cells to ferroptosis. *Exp. Hematol. Oncol.* **2023**, *12* (1), No. 47, DOI: 10.1186/s40164-023-00411-4.
(35) Khodakarami, A.; Kashani, M. A.; Nazer, A.; Kheshti, A. M.; Rashidi, B.; Karpisheh, V.; Masjedi, A.; Abolhasani, S.; Izadi, S.; Bagherifar, R.; Hejazian, S. S.; Mohammadi, H.; Movassaghpour, A.; Feizi, A. A. H.; Hojjat-Farsangi, M.; Jadidi-Niaragh, F. Targeted Silencing of NRF2 by rituximab-conjugated nanoparticles increases the sensitivity of chronic lymphoblastic leukemia cells to Cyclophosphamide. *Cell Commun. Signaling* **2023**, *21* (1), No. 188, DOI: 10.1186/s12964-023-01213-1.
(36) Watson, C. T.; Cohain, A. T.; Griffin, R. S.; Chun, Y.; Grishin, A.; Hacyznska, H.; Hoffman, G. E.; Beckmann, N. D.; Shah, H.; Dawson, P.; Henning, A.; Wood, R.; Burks, A. W.; Jones, S. M.; Leung, D. Y. M.; Sicherer, S.; Sampson, H. A.; Sharp, A. J.; Schadt, E. E.; Bunyavanich, S. Integrative transcriptomic analysis reveals key drivers of acute peanut allergic reactions. *Nat. Commun.* **2017**, *8* (1), No. 1943, DOI: 10.1038/s41467-017-02188-7.
(37) Cao, Y.; Huang, F.; Liu, J.; Qi, H.; Xiao, J. MiR-129−5p/TRIP13 affects malignant phenotypes of colorectal cancer cells. *Histol. Histopathol.* **2022**, *37*, 879 DOI: 10.14670/HH-18-455.
(38) Agarwal, S.; Afaq, F.; Bajpai, P.; Kim, H. G.; Elkholy, A.; Behring, M.; Chandrashekar, D. S.; Diffalha, S. A.; Khushman, M.; Sugandha, S. P.; Varambally, S.; Manne, U. DCZ0415, a small-molecule inhibitor targeting TRIP13, inhibits EMT and metastasis via inactivation of the FGFR4/STAT3 axis and the Wnt/beta-catenin pathway in colorectal cancer. *Mol. Oncol.* **2022**, *16* (8), 1728−1745.
(39) Chen, Y.; Chen, D.; Qin, Y.; Qiu, C.; Zhou, Y.; Dai, M.; Li, L.; Sun, Q.; Jiang, Y. TRIP13, identified as a hub gene of tumor progression, is the target of microRNA-4693−5p and a potential therapeutic target for colorectal cancer. *Cell Death Discovery* **2022**, *8* (1), No. 35, DOI: 10.1038/s41420-022-00824-w.
(40) Lu, R.; Zhou, Q.; Ju, L.; Chen, L.; Wang, F.; Shao, J. Upregulation of TRIP13 promotes the malignant progression of lung cancer via the EMT pathway. *Oncol. Rep.* **2021**, *46* (2), No. 172, DOI: 10.3892/or.2021.8123.
(41) Sheng, N.; Yan, L.; Wu, K.; You, W.; Gong, J.; Hu, L.; Tan, G.; Chen, H.; Wang, Z. TRIP13 promotes tumor growth and is associated with poor prognosis in colorectal cancer. *Cell Death Dis.* **2018**, *9* (3), No. 402, DOI: 10.1038/s41419-018-0434-z.
(42) Dong, L.; Ding, H.; Li, Y.; Xue, D.; Li, Z.; Liu, Y.; Zhang, T.; Zhou, J.; Wang, P. TRIP13 is a predictor for poor prognosis and regulates cell proliferation, migration and invasion in prostate cancer. *Int. J. Biol. Macromol.* **2019**, *121*, 200−206.
(43) Banerjee, R.; Russo, N.; Liu, M.; Basrur, V.; Bellile, E.; Palanisamy, N.; Scanlon, C. S.; van Tubergen, E.; Inglehart, R. C.; Metwally, T.; Mani, R. S.; Yocum, A.; Nyati, M. K.; Castilho, R. M.; Varambally, S.; Chinnaiyan, A. M.; D'Silva, N. J. TRIP13 promotes


https://doi.org/10.1021/acsomega.4c03450
*ACS Omega* 2024, 9, 26628−26640

error-prone nonhomologous end joining and induces chemoresistance in head and neck cancer. *Nat. Commun.* **2014**, *5*, No. 4527, DOI: 10.1038/ncomms5527.
(44) Tao, Y.; Yang, G.; Yang, H.; Song, D.; Hu, L.; Xie, B.; Wang, H.; Gao, L.; Gao, M.; Xu, H.; Xu, Z.; Wu, X.; Zhang, Y.; Zhu, W.; Zhan, F.; Shi, J. TRIP13 impairs mitotic checkpoint surveillance and is associated with poor prognosis in multiple myeloma. *Oncotarget* **2017**, *8* (16), 26718−26731.
(45) Ghosh, S.; Mazumdar, T.; Xu, W.; Powell, R. T.; Stephan, C.; Shen, L.; Shah, P. A.; Pickering, C. R.; Myers, J. N.; Wang, J.; Frederick, M. J.; Johnson, F. M. Combined TRIP13 and Aurora kinase inhibition induces apoptosis in human papillomavirus-driven cancers. *Clin. Cancer Res.* **2022**, *28*, 4479 DOI: 10.1158/1078-0432.CCR-22-1627.
(46) Liu, X.; Shen, X.; Zhang, J. TRIP13 exerts a cancer-promoting role in cervical cancer by enhancing Wnt/beta-catenin signaling via ACTN4. *Environ. Toxicol.* **2021**, *36* (9), 1829−1840.
(47) Hu, L.; Shi, J.; Shen, D.; Zhai, X.; Liang, D.; Wang, J.; Xie, C.; Xia, Z.; Cui, J.; Liu, F.; Du, S.; Meng, S.; Piao, H. Osimertinib induces paraptosis and TRIP13 confers resistance in glioblastoma cells. *Cell Death Discovery* **2023**, *9* (1), No. 333, DOI: 10.1038/s41420-023-01632-6.
(48) Xiao, Z.; Li, M.; Zhang, X.; Rong, X.; Xu, H. TRIP13 overexpression promotes gefitinib resistance in non-small cell lung cancer via regulating autophagy and phosphorylation of the EGFR signaling pathway. *Oncol. Rep.* **2023**, *49* (5), No. 84, DOI: 10.3892/or.2023.8521.
(49) Zhou, K.; Zhang, W.; Zhang, Q.; Gui, R.; Zhao, H.; Chai, X.; Li, Y.; Wei, X.; Song, Y. Loss of thyroid hormone receptor interactor 13 inhibits cell proliferation and survival in human chronic lymphocytic leukemia. *Oncotarget* **2017**, *8* (15), 25469−25481.
(50) Li, C.; Xia, J.; Franqui-Machin, R.; Chen, F.; He, Y.; Ashby, T. C.; Teng, F.; Xu, H.; Liu, D.; Gai, D.; Johnson, S. K.; van Rhee, F.; Janz, S.; Shaughnessy, J. D., Jr.; Tricot, G.; Frech, I.; Zhan, F. TRIP13 modulates protein deubiquitination and accelerates tumor development and progression of B cell malignancies. *J. Clin. Invest.* **2021**, *131* (14), No. e146893, DOI: 10.1172/JCI146893.
(51) Garcia, M. R.; Meissburger, B.; Chan, J.; de Guia, R. M.; Mattijssen, F.; Roessler, S.; Birkenfeld, A. L.; Raschzok, N.; Riols, F.; Tokarz, J.; Giroud, M.; Gil Lozano, M.; Hartleben, G.; Nawroth, P.; Haid, M.; Lopez, M.; Herzig, S.; Berriel Diaz, M. Trip13 Depletion in Liver Cancer Induces a Lipogenic Response Contributing to Plin2-Dependent Mitotic Cell Death. *Adv. Sci.* **2022**, *9*, No. e2104291, DOI: 10.1002/advs.202104291.
(52) Dong, L.; Ding, H.; Li, Y.; Xue, D.; Liu, Y. LncRNA TINCR is associated with clinical progression and serves as tumor suppressive role in prostate cancer. *Cancer Manage. Res.* **2018**, *10*, 2799−2807.
(53) Wang, Y.; Dong, S.; Hu, K.; Xu, L.; Feng, Q.; Li, B.; Wang, G.; Chen, G.; Zhang, B.; Jia, X.; Xu, Z.; Gao, X.; Zhang, H.; Xie, Y.; Lu, M.; Chang, S.; Song, D.; Wu, X.; Jia, Q.; Zhu, H.; Zhou, J.; Zhu, W.; Shi, J. The novel norcantharidin derivative DCZ5417 suppresses multiple myeloma progression by targeting the TRIP13-MAPK-YWHAE signaling pathway. *J. Transl. Med.* **2023**, *21* (1), No. 858, DOI: 10.1186/s12967-023-04739-7.
(54) Dong, S.; Hu, K.; Shi, Y.; Wang, G.; Yu, D.; Zhao, Y.; Zhang, H.; Wang, Y.; Sun, H.; Xu, Z.; Jia, Q.; Li, Y.; Li, Y.; Li, B.; Shi, J.; Zhu, W. Design and synthesis of cantharidin derivative DCZ5418 as a TRIP13 inhibitor with anti-multiple myeloma activity in vitro and in vivo. *Bioorg. Med. Chem. Lett.* **2024**, *98*, No. 129590.
(55) Wang, Y.; Huang, J.; Li, B.; Xue, H.; Tricot, G.; Hu, L.; Xu, Z.; Sun, X.; Chang, S.; Gao, L.; Tao, Y.; Xu, H.; Xie, Y.; Xiao, W.; Yu, D.; Kong, Y.; Chen, G.; Sun, X.; Lian, F.; Zhang, N.; Wu, X.; Mao, Z.; Zhan, F.; Zhu, W.; Shi, J. A Small-Molecule Inhibitor Targeting TRIP13 Suppresses Multiple Myeloma Progression. *Cancer Res.* **2020**, *80* (3), 536−548.
(56) Banerjee, R.; Liu, M.; Bellile, E.; Schmitd, L. B.; Goto, M.; Hutchinson, M. N. D.; Singh, P.; Zhang, S.; Damodaran, D. P. V.; Nyati, M. K.; Spector, M. E.; Ward, B.; Wolf, G.; Casper, K.; Mierzwa, M.; D'Silva, N. J. Phosphorylation of TRIP13 at Y56 induces radiation resistance but sensitizes head and neck cancer to cetuximab. *Mol. Ther.* **2022**, *30* (1), 468−484.
(57) Nepstad, I.; Hatfield, K. J.; Gronningsaeter, I. S.; Reikvam, H. The PI3K-Akt-mTOR Signaling Pathway in Human Acute Myeloid Leukemia (AML) Cells. *Int. J. Mol. Sci.* **2020**, *21* (8), No. 2907, DOI: 10.3390/ijms21082907.


https://doi.org/10.1021/acsomega.4c03450
*ACS Omega* 2024, 9, 26628−26640